Sphingomyelin at the air–water interface

David Vaknin[a] and Michael S. Kelley
Ames Laboratory and Department of Physics and Astronomy, Iowa State University, Ames, Iowa 50011

Benjamin M. Ocko
Department of Physics, Brookhaven National Laboratory, Upton, New York 11973

(Received 13 June 2001; accepted 7 August 2001)

X-ray reflectivity (XR) and grazing incident-angle x-ray diffraction (GIXD) reveal that sphingomyelin, although forming homogeneous monomolecular films at air–water interfaces, does not develop long-range crystalline in-plane order at any in-plane density, most notably at high surface pressures where many other membrane lipids order as two-dimensional crystals. Studies were carried out on the monodisperse synthetic C18-sphingomyelin where both hydrocarbon chains are saturated and on natural sphingomyelin which contains a distribution of chain lengths, with saturated and unsaturated hydrocarbon chains. The surface pressure versus molecular area (π–A) isotherm for the natural sphingomyelin is similar to that of the synthetic, but has a somewhat higher surface pressure at intermediate areas. The absence of in-plane crystalline order is attributed to competing interactions in the head group region: hydrogen bonding in the erythro region, electrostatic interactions among zwitterions of neighboring head groups, and van der Waals among acyl chains. © *2001 American Institute of Physics.* [DOI: 10.1063/1.1406501]

I. INTRODUCTION

Lipids are well known to have important if rather passive functions in the cell. They are the primary components of plasma and organelle membranes which in turn form permeability barriers and provide appropriate environments for the action of membrane proteins. However, beyond these passive roles certain lipids, such as sphingolipids, actively participate in the life cycle of living cells. Sphingosine, from which sphingolipids are derived, is an amino alcohol that contains long, unsaturated acyl chain, and it mediates cell proliferation.[1–3] On the other hand, ceramide, an N-acylated sphingosine derivative, acts as a second messenger by stimulating proteins (kinase and phosphatase) that regulate cell growth and apoptosis.[2] Sphingomyelin (SPM), a ceramide derived phospholipid with a phosphorylcholine (PC) moiety, is abundant in the myelin sheath that serves as an insulator around nerve fibers, but it is also a common component of plasma membranes, subcellular organelle, and mitochondria. SPM metabolically recycles in a process that involves the removal of the PC moiety by sphingomyelinase, yielding ceramide which in turn can be transformed into sphingosine in the so-called *sphingomyelin cycle*.[1]

Naturally occurring sphingomyelin (N-SPM) is heterogeneous, consisting of a variety of amide-linked fatty acids of which the predominant ones are: stearic acid (C18-SPM; 45%) which is saturated, and lignoceric acid (C24-SPM; 31%) which has *cis*-double bond in the middle of the chain. Thus, through the metabolic SPM cycle sphingomyelin molecules yield a variety of ceramides with amide-linked fatty-acids that vary in length and saturation and consequently in their physiologic functionality.[2,3] Monodisperse SPMs, such as C18-SPM or C16-SPM, can be readily synthesized or purified, and their bulk properties have been studied. X-ray diffraction and calorimetric studies of a variety of synthetic monodisperse SPMs were conducted and compared to those of N-SPM.[4,5] Those studies demonstrated that some of the complex behavior of N-SPM can be attributed to the heterogeneity in their amide-linked fatty acid composition.[5] In the present study, we compare the behavior of C18-SPM and N-SPM as monolayers that are spread at the air–water interface, to examine how the acyl-chain distribution, both chain length and degree of saturation, affect the in-plane packing of the films, and also examine to what extent structural properties of natural SPM can be approximated by those of pure C18-SPM.

Structural studies of oriented N-SPM bilayers yielded a lamellar repeat unit for the bilayer $d=68.5$ Å with very little if any interdigitation of hydrocarbon chains, and also showed that the bilayer did not swell when exposed to high humidities.[6] Furthermore, an in-plane reflection due to hydrocarbon chains packing (4.2 Å) indicated that the chains are at right angles to the bilayer surface with in-plane disorder. In those studies, the comparison of the Patterson functions of SPM with those of dipalmitoyl-phosphatidyl choline (DPPC) suggested that structural features of SPM in oriented bilayers resemble those of DPPC. However, other studies indicated prominent differences in the net dipole moments of DPPC and SPM and in their ability to form hydrogen bonds.[6,7] We have undertaken the present x-ray study to determine the structural differences between SPM and DPPC in monolayers at aqueous interfaces where electrostatic interactions among zwitterions in the head group, and hydrogen bonding are readily expressed resembling cellular environment. To examine the effect of the sphingosine head group, we have also compared SPM results with those of C18-ceramide monolayers.[8]

[a]Electronic mail: vaknin@ameslab.gov

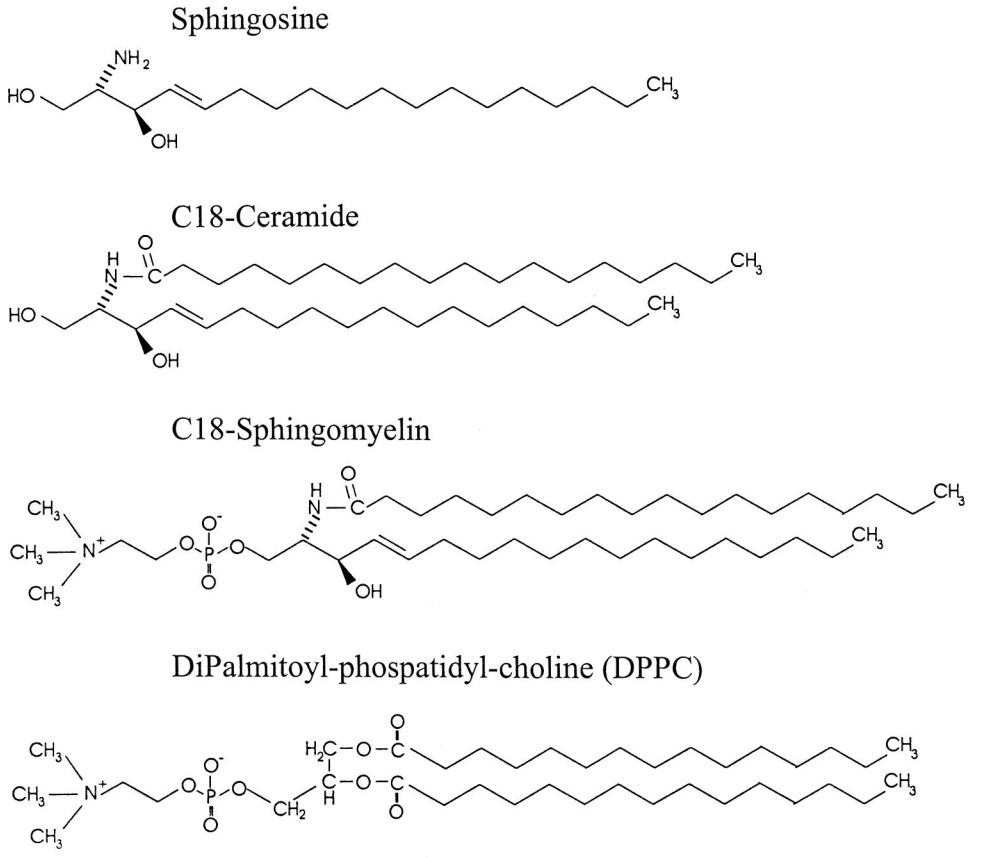

FIG. 1. The molecules used in this study. In the naturally occurring sphingomyelin, N-SPM the amide-linked fatty acid varies with the following main composition: C16:0 3%; C18:0 45%; C20:0 1%; C22:0 4%; C24:0 8%; C24:1 31% and others.

II. EXPERIMENTAL DETAILS

A. Materials and Langmuir trough

Natural sphingomyelin (N-SPM) (see Fig. 1) from bovine brain and C18-SPM (N-octadecanoyl-sphingosyl-phosphorylcholine) were obtained from Matreya, Inc. (Pleasant Gap, PA) (materials have catalog numbers 1051 and 1911, respectively, in the Matreya, Inc. Catalog # 7, 1999–2000) with an average MW of 749. The ceramide sample C18-ceramide was also obtained from Matreya, Inc., and was used in previous studies.[8] L-α-dipalmitoyl-phosphatidylcholine (DPPC C16:0) was purchased from Sigma Chemical Co. (St. Louis, MO). Samples were weighed directly into volumetric flasks and were subsequently filled with chloroform (HPLC grade, Fisher Scientific, Fair Lawn, NJ) and sonicated to form uniform solutions. Langmuir monolayers were prepared on pure water (Milli-Q apparatus Millipore Corp., Bedford, MA; resistivity, 18.2 MΩcm) in a temperature-controlled Teflon trough maintained at $18\pm1\,^{\circ}\mathrm{C}$ in a gas-tight aluminum container. Surface pressure (π) was measured with a microbalance using a filter-paper Wilhelmy plate. To reduce incoherent scattering from air, and to slow film deterioration by oxidation due to production of radicals by the intense synchrotron beam, the monolayer was kept under a He environment during the x-ray measurements. No noticeable differences were found in the $\pi-A$ isotherms when performed under air or He environments.

B. X-ray scattering

In situ x-ray scattering experiments from the monolayers at the air–water interface were carried out on the Harvard/BNL Liquid Surface Diffractometer at the National Synchrotron Light Source (NSLS), beamline X22B with a wavelength $\lambda=1.54$ Å (described elsewhere[9]). Specular XR experiments are conducted to determine the electron density profiles across the interface and to relate them to molecular arrangements in the film. To extract the electron density profiles from the measured reflectivity, a slab model is constructed and refined by the nonlinear least-squares method. The reflectivity from the slab model at a momentum transfer Q_z is calculated as follows:

$$R(Q_z)=R_0(Q_z)e^{-(Q_z\sigma)^2}, \tag{1}$$

where $R_0(Q_z)$ is the reflectivity from step-like functions calculated by the recursive dynamical method,[10] and σ is an effective surface roughness, accounting for the smearing of all interfaces (conformal surface roughness) due to thermal capillary waves and surface inhomogeneities.[11,12] The variable parameters used to construct the electron density across the interface $\rho(z)$ include the thicknesses of the various slabs, their electron densities, and one surface roughness. The number of slabs used to fit the data is the minimum necessary for which an additional slab does not improve the quality of the fit.

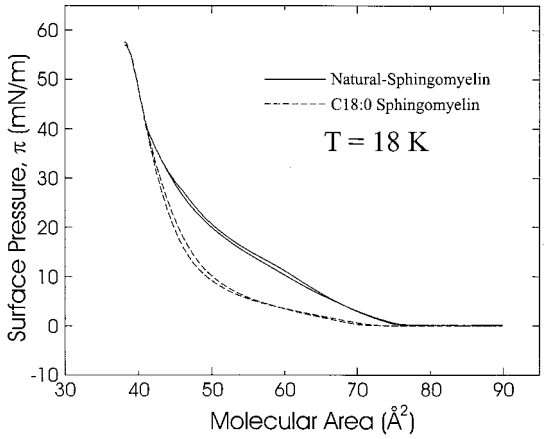

FIG. 2. $\pi-A$ isotherms for N-SPM and C18-SPM at $T=18\,^{\circ}\mathrm{C}$. The two curves for each material represent the reproducibility of the isotherms from different preparations. It is argued that the presence of *cis*-double-bond of N-SPM (C24:1 31%) is the main cause for the difference between the isotherms of C18-SPM and N-SPM.

Grazing incident-angle x-ray diffraction experiments (GIXD) were used to determine the lateral organization in the film. In these experiments, the angle of the incident beam with the surface α is fixed below the critical angle for total reflection while the diffracted beam is detected at a finite in-plane angle 2θ. The resolution function of the diffractometer $G(Q_{xy})$ was convolved with the intrinsic line shape of the model 2D Bragg peak $S(Q_{xy})$ to fit the observed diffraction pattern as follows:

$$I(Q_{xy})=\int G(Q'_{xy})S(Q'_{xy}-Q_{xy})dQ'_{xy}. \tag{2}$$

To obtain the structure factor of the diffracting entities $F(Q_z)$ scans along the out-of-plane angle β at the Bragg peak position (rod scans) were measured with a linear position sensitive detector (PSD), and analyzed using standard procedures.[12,13] The intensity along the rod of the 2D Bragg reflection was analyzed in the framework of the distorted wave Born approximation (DWBA) using[12,15]

$$I\propto|t(k_{z,i})|^2|F(Q_z)|^2e^{-(Q_z\sigma_{\mathrm{eff}})^2}|t(k_{z,f})|^2, \tag{3}$$

where $t(k_{z,f})$, and $t(k_{z,i})$ are the Fresnel transmission functions which give rise to an enhancement around the critical angle.

III. RESULTS AND ANALYSIS

A. $\pi-A$ isotherms

Figure 2 shows surface pressure versus molecular area ($\pi-A$) isotherm for N-SPM (solid line) and C18-SPM (dashed line) at $T=18\,^{\circ}\mathrm{C}$ on pure water. The two $\pi-A$ curves for C18-SPM and for N-SPM were obtained from different samples to demonstrate the degree of reproducibility of the isotherms. The initial rise in surface pressure, at ≈ 75 Å^2 occurs at a higher surface area for N-SPM compared to the C18-SPM monolayer, and the surface pressure remains higher at intermediate surface areas. Close to the collapse, at about 40 Å^2 both curves are nearly identical. Isotherms of phospholipids are usually marked by two sharp features. The first occurs at relatively large molecular areas, at a pressure π_c. It indicates an onset of transformation from liquid-expanded (LE) to the mixed phase LE/LC (LC stands for liquid-condensed), and it is temperature dependent. The second feature occurs at molecular areas of closely packed hydrocarbon chains, at π_s, and it resembles a transition due to chain crystallization of simple fatty acids at air–water interfaces.[16] The $\pi-A$ isotherms of the monodisperse C18-SPM and N-SPM are smooth with no sharp features characteristic of the two transitions mentioned above. The difference between the isotherms of the two systems can be ascribed to the presence of *cis*-double bond in the amine-linked alkyl chain (C24:1 lignoceric) which is a component in about 31% of the molecules (that is, about 15% of the total number chains in the film) as discussed below.

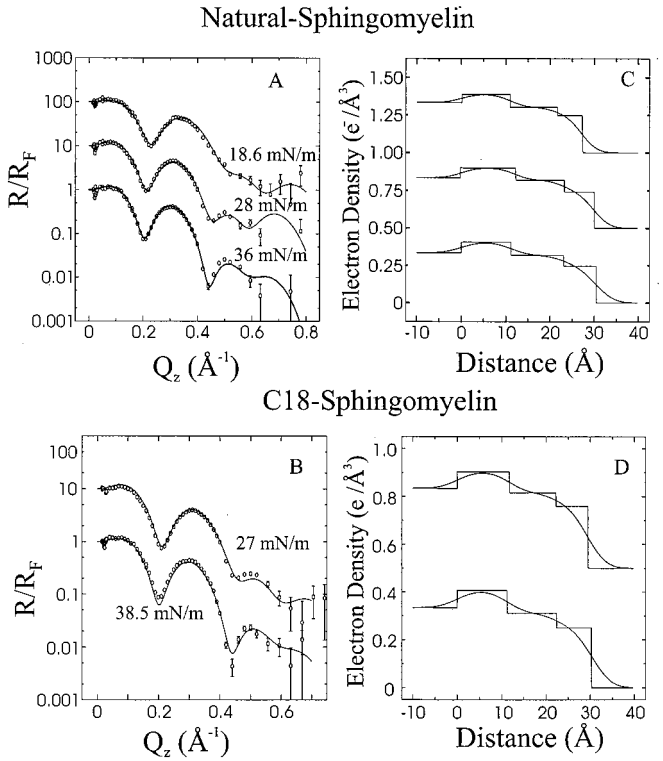

FIG. 3. Normalized reflectivity curves from monolayers of N-SPM and C18-SPM (A and B, respectively). Solid lines are calculated reflectivities based on the corresponding electron density profiles shown in C and D.

B. X-ray reflectivity

Figures 3(A) and 3(B) show measured reflectivity curves that are normalized to the calculated reflectivity of ideally flat water interface R_F for both the C18-SPM and N-SPM monolayers. The three-slab model is used to fit the data, where the slab contiguous to the aqueous subphase is associated with the lipid head group and integrated water molecules, and the second and third slabs, at the air interface, consist of the acyl chains. The solid lines in Figs. 3(A) and 3(B) are the best fits to the data using the corresponding electron densities shown in Figs. 3(C) and 3(D), respectively. These three-slab models indicate that the electron density

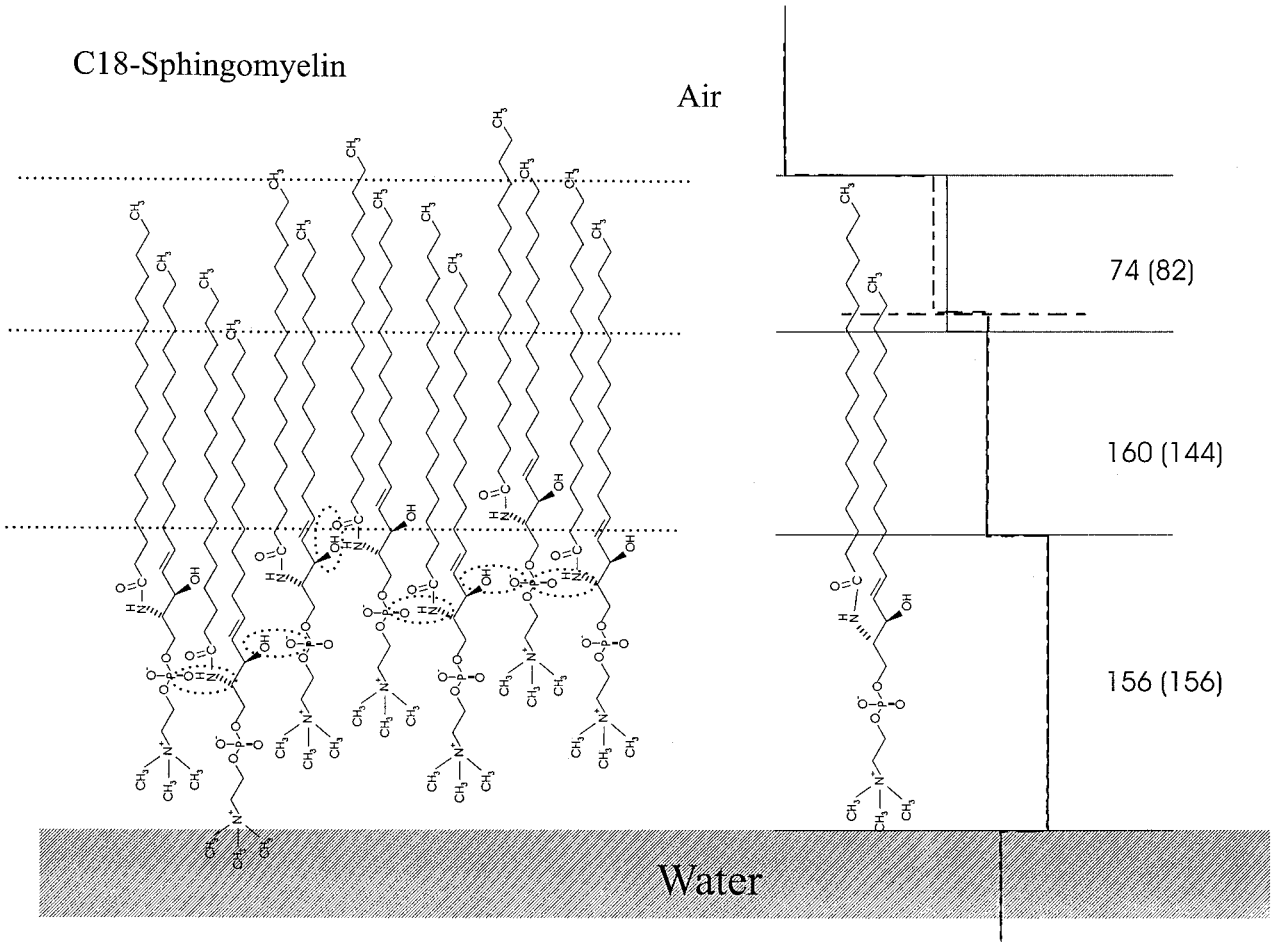

FIG. 4. Schematic association of molecular moieties with the slab model of the electron density as determined from the reflectivity curves. The interfaces in the model are associated with the average locations on the molecule, but may differ slightly from one site to another, as shown schematically to the left. It is argued that the nearest-neighbor molecules are located at different positions with respect to the ideally flat water surface due to strong hydrogen bonding among different parts of neighboring head groups (possible H bonds are circled with dashed lines). This leads to the observation of two slabs associated with the acyl chains and also to the observed short-range in-plane order.

along the hydrocarbon-chain region of the molecule is not uniform, consisting of at least two distinct densities, as is schematically depicted in Fig. 4. In order to associate molecular sections with the slab model, we used the space-filling refinement procedures.[8,14] The thicknesses of the three slabs, surface roughness, and the number of water molecules in the head group region, are the variable parameters in this procedure. The electron density of each slab is determined from the molecular constituents, and the volume they occupy, which is calculated from the molecular area and the thickness of the slab.[14] These variable parameters together with the constants are listed in Table I for the pure C18-SPM and in Table II for the N-SPM extract. In general, the reflectivities of C18-SPM and N-SPM are practically indistinguishable, yielding the same structural parameters within the experimental uncertainty range. This suggests that the *cis*-bond present among 15% of acyl chains does not significantly affect the average electron density profile of N-SPM. As the monolayers are compressed to higher surface pressures, two trends are noticeable. First, the average number of water molecules in the head group region is getting smaller; water molecules are ''squeezed out'' of the head group region. Second, surface roughness slightly increases with the pressure. We argue that this increase in surface roughness and the division of the acyl chain layer into two distinct layers come about as a result of the fact that molecules in the monolayer are located at different heights with respect to the water surface, as discussed below (see Fig. 4).

C. GIXD and rod scans from the monolayer

At finite pressures, GIXD scans versus in-plane scattering vector in the range $0.1 \leqslant Q_{xy} \leqslant 2.0$ Å^{-1} revealed a single broad peak in a Q_{xy} range that indicates the 2D ordering of the hydrocarbon chains (d spacing ≈ 4.2 Å). Figure 5 shows the diffraction pattern from the monolayers for different lateral pressures, with a prominent peak at $Q_{xy}^0 \approx 1.437$ Å^{-1}. Similar scans at smaller angles did not reveal any detectable lower order reflections that could be assigned to the ordering of the molecular head groups. Also, no extra peaks off the horizon at finite Q_z were observed. These usually come about as a result of a broken hexagonal symmetry due to the tilting of the hydrocarbon chains with respect to the surface normal. Monolayers of DPPC, as our study confirms, order in the oblique symmetry exhibiting three diffraction peaks one at the horizon $(1\bar{1})$ and another two off the horizon

TABLE I. Best-fit parameters used in the three-slab model for the reflectivity of C18-SPM monolayer on H_2O.

Pressure	27 mN/m	38.5 mN/m	
Independent variables			
$d_{\text{tail},2}$ (Å)	7.3±0.7	8.0±0.7	Thickness of upper tail slab
$d_{\text{tail},1}$ (Å)	10.5±0.6	11.3±0.7	Thickness of intermediate tail slab
d_{head} (Å)	11.7±0.6	11.2±0.8	Head group layer thickness
$N_{\text{H}_2\text{O,head}}$	4.9±1.8	3.02±2.1	Number of water molecules in head group
σ (Å)	3.3±0.1	3.4±0.1	Interfacial roughness
Dependent variables			
$\rho_{\text{tail},2}$ (e/Å^3)	0.260±0.010	0.250±0.009	Electron density of upper tail slab
$\rho_{\text{tail},1}$ (e/Å^3	0.315±0.025	0.311±0.027	Electron density of intermediate tail slab
ρ_{head} (e/Å^3)	0.40±0.001	0.40±0.001	Electron density of head group slab
d_{total} (Å)	29.5±1.3	30.5±1.6	Total thickness of interfacial layer
Constants			
A_m (Å^2)	43.5±1	41±1	Molecular area (from isotherm)
$N_{e,\text{tail},2}$	82		Electrons in upper tail slab
$N_{e,\text{tail},1}$	144		Electrons in intermediate tail slab
$N_{e,\text{head}}$	156		Electrons in head group slab
$N_{e,\text{H}_2\text{O}}$	10		Electrons per water molecule

labeled (10) and (01) (which overlap one another, giving rise to a broad peak at finite Q_z).[17] The $(1\bar{1})$ peak of the DPPC monolayer at high π is nearly resolution limited, yielding a correlation length that is greater than 600 Å. A similar correlation length is obtained for C18-ceramide. The most striking feature in the GIXD of C18-SPM and N-SPM monolayers is the considerably broad linewidth at high surface pressures. Assuming that the in-plane correlation length decays exponentially, the diffraction peak has a Lorentzian line shape

$$S(Q_{xy}) \sim \frac{C}{1+(\Delta Q/\kappa)^2}, \tag{4}$$

where $\Delta Q = Q_{xy} - Q_{xy}^0$, and κ=the linewidth, is inversely proportional to the in-plane correlation length. The fit to the data shown in Fig. 5 accounts for the resolution of the spectrometer by use of Eq. (4) with a Gaussian resolution function determined from the configuration of the spectrometer. Table III lists the diffraction parameters for SPM, DPPC, and C18-ceramide monolayers. Although the correlation length increases slightly upon increasing surface pressure, the monomolecular films (C18-SPM and N-SPM) do not develop long-range crystalline in-plane order at any in-plane density, most notably at high surface pressures where many other membrane lipids order as two-dimensional crystals.

The observation of a single diffraction peak due to the ordering of saturated chains suggests that the 15% *cis*-double bond chains are most likely completely disordered. That, together with the fact that the correlation lengths for C18-SPM and N-SPM are practically the same, implies that the lignoceric component in the monolayer phase separates from the saturated chain environment formed by the other constituents of N-SPM. If those 15% *cis*-double-bond present were miscible among the saturated chains we would have observed a significant decrease in the correlation length of N-SPM compared to that of C18-SPM.

The intensity along the rod of the 2D Bragg reflection (see Fig. 5) is analyzed using Eq. (3), and the following

TABLE II. Best-fit parameters used in the three-slab model for the reflectivity of N-SPM monolayer on H_2O.

Pressure	18.5 mN/m	28 mN/m	36 mN/m	
Independent variables				
$d_{\text{tail},2}$ (Å)	5.9±0.5	6.8±0.5	7.2±0.5	Thickness of upper tail slab
$d_{\text{tail},1}$ (Å)	10.4±0.7	11.2±0.7	12.0±0.7	Thickness of intermediate tail slab
d_{head} (Å)	11.0±0.5	12.0±0.7	11.2±0.7	Head group layer thickness
$N_{\text{H}_2\text{O,head}}$	6.2±1.6	6.0±1.9	3.6±2.1	Number of water molecules in head group
σ (Å)	2.8±0.1	2.8±0.1	3.25±0.15	Interfacial roughness
Dependent variables				
$\rho_{\text{tail},2}$ (e/Å^3)	0.250±0.008	0.240±0.007	0.245±0.008	Electron density of upper tail slab
$\rho_{\text{tail},1}$ (e/Å^3)	0.302±0.024	0.317±0.025	0.317±0.025	Electron density of intermediate tail slab
ρ_{head} (e/Å^3)	0.389±0.006	0.400±0.007	0.408±0.008	Electron density of head group slab
d_{total} (Å)	27.3±1.3	30.0±1.5	30.4±1.6	Total thickness of interfacial layer
Constants				
A_m (Å^2/Molecule)	51.0±1	45.0±1	42.0±1	Sphingomyelin area from isotherm
$N_{e,\text{tail},2}$	74			Electrons in short tail per molecule
$N_{e,\text{tail},1}$	160			Electrons in long tail per molecule
$N_{e,\text{head}}$	156			Electrons in head group per molecule
$N_{e,\text{H}_2\text{O}}$	10			Electrons per water molecule

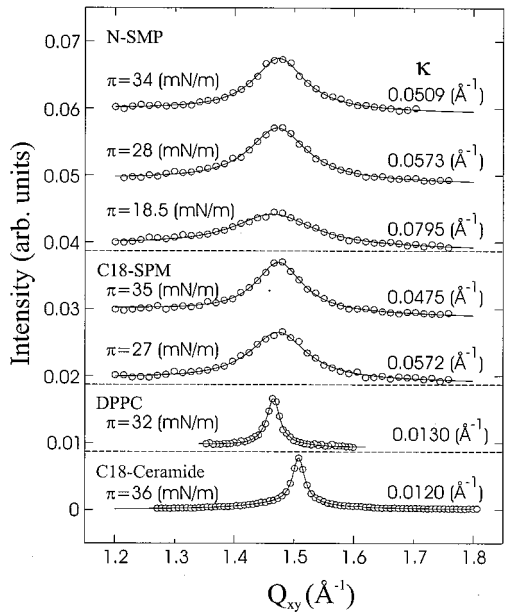

FIG. 5. Diffraction patterns from an N-SPM, C18-SPM DPPC, and C18-ceramide. The prominent 2D Bragg reflection is due to the saturated acyl chain ordering, which can be used to probe lateral correlation lengths in the monolayer. The diffraction pattern of N-SPM is dominated by the scattering from the saturated amide-linked hydrocarbon chains. We argue that the lignoceric-SPM (C24:1; 31% with a kink in the center of the chain) component in N-SPM, phase separates from the other components of N-SPM and is completely disordered, therefore not contributing to significant differences in the GIXD between N-SPM and C18-SPM.

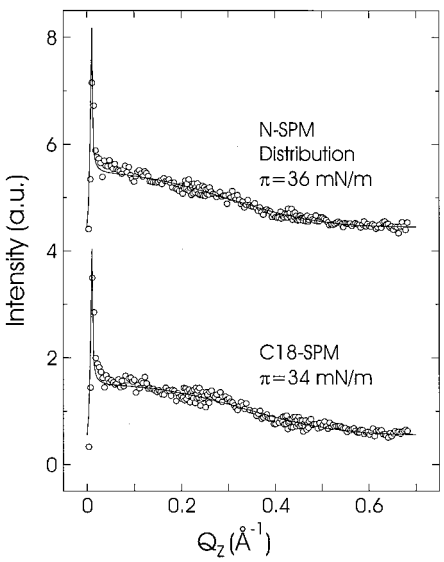

FIG. 6. Rod scans from N-SPM and C18-SPM indicating a very small tilt of the hydrocarbon chains with respect to the surface normal, consistent with the reflectivity results.

structure factor for an alkyl chain with length d:[18]

$$F(Q_z')=\frac{\sin(Q_z'd/2)}{Q_z'd/2}, \tag{5}$$

where Q_z' is defined in a frame in which the z axis is parallel to the chain of the molecule. In our model, it is assumed that each chain can be tilted with respect to the surface normal either towards the nearest neighbor (NN) or towards next-nearest neighbor (NNN).[13,18] The solid lines in Fig. 6 are the best fit to the data using tilt angles as variable parameters, and assuming that the ordered region of the hydrocarbon chains is the central section of the acyl-chain layer as obtained from the reflectivity ($d_{\text{tail},1}\sim 11.5$ Å), as listed in Table IV. The fits to the rod scans were found to be insensitive to the tilt direction.

IV. DISCUSSION

A. Molecular interpretation of the electron density profile across the interface

In simple terms, the electron density profile (Fig. 3) can be related to the organization of the molecules at the interface by calculating the average total number of electrons per molecule N_{total} as follows:

$$N_{\text{total}}=A_m\int \rho(z)dz=A_m\sum_j \rho_j d_j, \tag{6}$$

where the molecular area A_m can be obtained either from the isotherm or from the in-plane Bragg reflection.[8] Equation (6) for C18-SPM at 27 mN/m yields $\approx$430 electrons, compared with 382 electrons associated with the empirical formula of C18-SPM. The difference between these two numbers is attributed to the inclusion of bound water molecules (approximately five), in the head group region, as listed in Table I. Also, our analysis shows that with the increase of pressure the number of water molecules in the head group region decreases. Based on Tables I and II a proposed division of the molecule into different slabs is shown in Fig. 4. In recent x-ray reflectivity studies of ceramide and sphingosine it was

TABLE III. Best-fit in-plane peak positions and width, the correlation length ξ, and the cross section per acyl chain in the plane normal to the acyl chain axis A_0.

	π (mN/m)	GID peak (Å^{-1})	Width (Å^{-1})	ξ (Å)	d spacing (Å)	A_0 (Å^2)
Sphingomyelin distribution	34	1.475	0.051	123.0	4.260	20.95
	27	1.473	0.057	110.0	4.266	21.01
	18.5	1.465	0.080	79.0	4.289	21.24
C_{18} sphingomyelin	35	1.475	0.048	131.0	4.260	20.95
	27	1.474	0.057	110.0	4.263	20.98
DPPC	32	1.466	0.010	628	4.286	20.3
C_{18} ceramide	36	1.508	0.013	483	4.167	20.05

TABLE IV. Parameters for fitting the rod scans from sphingomyelin monolayers. Two tilt directions were examined, one towards nearest neighbors and another towards next-nearest neighbors. The quality of the fit was insensitive to the tilt direction of the chains.

	C18-SPM	N-SPM	
Variables			
θ (deg)	$5.4\pm^{6.0}_{4.5}$	$4.2\pm^{5.0}_{2.4}$	Tilt from surface normal
Constants			
$d_{\text{tail},1}$ (Å)	11.3	12.0	Length of diffracting object
Q_{xy} (Å^{-1})	1.48	1.48	

argued that nearest-neighbor sphingolipids tend to stagger along the surface normal, giving rise to a corrugated head group slab,[8] and conforming to it a corrugated acyl-chain layer at the air interface. Such randomly corrugated interface is also the cause for the increased surface roughness at high pressures. Strong hydrogen bonding between the amide carbonyl of one molecule and the hydroxyl group or the phosphoryl of another, can bind two neighboring molecules at different positions with respect to the water interface, giving rise to the inhomogeneity associated with the film, as shown schematically in Fig. 4. NMR studies of SPM aggregates suggest strong hydrogen bonding between the sphingosine hydroxyl group and the phosphoryl which will create the proposed irregular corrugation.[19]

The total thickness of the acyl chains at high pressures ($\geqslant$25 mN/m) ~18.3–19.0 Å is very close in value to the total thickness of the acyl-chain slabs in C18-ceramide (19.02 Å), for which it was concluded that the tilt angle from the surface normal is negligible.[8] This is consistent with the analysis of the rod scans which yield an average tilt angle that is smaller than 5 deg.

B. In-plane disorder

Above π_c and below the solid phase, monolayers of phospholipids give rise to broad peaks associated with the ordering of the chains, implying short-range, in-plane order.[20–22] The correlation length increases gradually as the monolayer is compressed, and above π_s long-range order establishes. In that regard, the behavior of C18-SPM and N-SPM is very different from that of known phospholipids[20–22] as they do not develop long-range order at any pressure or density. The correlation length at the smallest molecular area ($\approx$41 Å^2) is finite, characteristic of an amorphous solid. By comparing to other phospholipids, in particular to DPPC, it can be ascertained that the PC portion in the head group by itself is not responsible for the short-range order observed. We argue that strong hydrogen bonding in the erythro and phosphoryl regions of the head group, coupled with strong electrostatic interactions, lock the molecules in irregular positions forcing the chains into a glassy, closely packed state. On the other hand, the heterogeneity in saturated amide-linked acyl chains has an insignificant effect, if any at all on the in-plane disorder, as the differences between C18-SPM and N-SPM are negligible (Fig. 5). Despite the in-plane disorder in the chain region, the chains are actually closely packed. This is evidenced from the area per molecule determined from the isotherms as well as from the unit cell per chain as determined from the GIXD. Also, the reflectivity results show that the electron density of the intermediate chain region is about 95% that of closely packed alkanes. The cross-section area of the acyl chains in the plane that is perpendicular to the average chain axis, A_0, as determined from the GIXD is approximately 21 Å^2, compared to 20.3 for DPPC[22] and 20.00 for C18-ceramide.[8] It is plausible that the larger area per chain in SPM provide sufficient space for the chains to tilt from the surface normal (average angle of 5 deg) at random orientation, which may manifest itself as the short-range order observed. The relatively small tilt from the surface normal is consistent with results from oriented bilayers which show that the chains are practically at right angles to the bilayer sheets.[23] This is in contrast to DPPC, where the tilt angle is about 30 deg at comparable surface pressures.

It is well known that mechanical strength of materials is enhanced as they become somewhat amorphous mainly due to the absence of distinct dislocations, or grain boundaries that tend to weaken crystalline materials.[24] The amorphous nature of SPM, as detected by the GIXD, suggests that the head groups are tightly bound and locally ordered, lacking the long-range order that introduces the weakening dislocations. Strong bonding at the head group slab gives the film the impermeability property required for the primary function of myelin membrane as an insulator, and at the same time enhances its mechanical strength. The lipid content in myelin membranes exceeds 80%, with 20% protein distributed randomly.

C. C18-SPM versus N-SPM

The reflectivity and the diffraction experiments both show that C18-SPM and N-SPM behave similarly on water surfaces. The isotherms, on the other hand, show significant differences between the two. We argue that the difference between the two π–A curves can be ascribed to the presence of *cis*-alkyl chain which is a component in about 31% of the molecules (that is, about 15% of the total number chains in the film). The effects of double bonds on the monolayer phase behavior have been investigated by Fehrer and co-workers[25] for C18 fatty acid monolayers and by Williams and co-workers for phospholipid monolayers.[26] For stearic acid (saturated chains) the initial pressure rise occurs at about 25 Å^2, whereas for oleic acid (unsaturated chains) it occurs at about 55 Å^2, nearly twice the molecular area of the densely packed film. This critical area suggests that for oleic acid the first nine carbon atoms lie nearly parallel to the water surface. For mixed monolayers of stearic and oleic acids, Fehrer and co-workers concluded that the saturated and unsaturated components are immiscible. Likewise, for mixed phospholipids monolayers William and co-workers found that demixing occurred when one of the chains in one of the components was saturated (DOPC and DPPG).[27] On the other hand, phospholipids with different head groups (DPPC and DPPG) but with the same chains were miscible.[26] The results of the present study suggest that the lignoceric component (31% C24:1) in N-SPM is not miscible in the rest of the saturated constituents leading to the differences in the π–A isotherms.

ACKNOWLEDGMENTS

Ames Laboratory is operated for the U.S. Department of Energy by Iowa State University under Contract No. W-7405-Eng-82. The work at Ames was supported by the Director for Energy Research, Office of Basic Energy Sciences.

[1] S. Spiegel and A. Merrill, FASEB J. **10**, 1388 (1996).
[2] Y. A. Hannun, J. Biol. Chem. **269**, 3125 (1994).
[3] J. M. Hauser, B. M. Buehrer, and R. M. Bell, J. Biol. Chem. **269**, 6803 (1994).
[4] P. R. Maulik and G. G. Shipley, Biophys. J. **69**, 1909 (1995).
[5] P. R. Maulik and G. G. Shipley, Biochemistry **35**, 8025 (1996).
[6] R. S. Khare and C. R. Worthington, Biochim. Biophys. Acta **514**, 239 (1978).
[7] D. O. Shah, and J. H. Schulman, Biochim. Biophys. Acta **135**, 184 (1967).
[8] D. Vaknin and M. S. Kelley, Biophys. J. **79**, 2616 (2000).
[9] D. K. Schwartz, M. L. Schlossman, and P. S. Pershan, J. Chem. Phys. **96**, 2356 (1992).
[10] L. G. Parratt, Phys. Rev. **59**, 359 (1954).
[11] J. Als-Nielsen and K. Kjaer, in *Phase Transitions in Soft Condensed Matter*, edited by T. Riste and D. Sherrington (Plenum, New York, 1989), p. 113.
[12] D. Vaknin, in *Methods in Materials Research*, edited by E. N. Kaufmann, R. Abbaschian, P. A. Barnes, A. B. Bocarsly, C.-L. Chien, B. L. Doyle, B. Fultz, L. Leibowitz, T. Mason, and J. M. Sanchez (Wiley, New York, 2001), p. 10d.2.1.
[13] K. Kjaer, Physica B **198**, 100 (1994).
[14] D. Vaknin, K. Kjaer, J. Als-Nielsen, and M. Lösche, Biophys. J. **59**, 1325 (1991).
[15] G. Vineyard, Phys. Rev. B **26**, 4146 (1982).
[16] O. Albrecht, H. Gruler, and E. Sackmann, J. Phys. (Paris) **39**, 301 (1978).
[17] U. Dahmen-Levison, G. Brezesinski, and H. Möhwald, Thin Solid Films **327–329**, 616 (1998).
[18] K. Kjaer, J. Als-Nielsen, C. A. Helm, P. Tippmann-Krayer, and H. Möhwald, J. Phys. Chem. **93**, 3200 (1989).
[19] K. S. Bruzik, Biochim. Biophys. Acta **939**, 315 (1988).
[20] C. A. Helm, H. Möhwald, K. Kjaer, and J. Als-Nielsen, Biophys. J. **52**, 381 (1987).
[21] C. A. Helm, P. Tippmann-Krayer, H. Möhwald, J. Als-Nielsen, and K. Kjaer, Biophys. J. **60**, 1457 (1991).
[22] G. Brezesinski, A. Dietrich, B. Struth, C. Böhm, W. G. Bouwman, K. Ljaer, and H. Möhwald, Chem. Phys. Lipids **76**, 145 (1995).
[23] The diffraction results of Khare *et al.* (Ref. 6) are consistent with about 3.5–4 deg tilt angle with respect to the layers' normal. Also, it is important to note that the Bragg peaks associated with the bilayer *d* spacing are significantly sharper than the one due to the chain in-plane ordering peak, despite the fact that the chains vary in lengths [see Fig. 1 (Ref. 6)].
[24] C. Kittel, *Introduction to Solid State Physics*, 6th ed. (Wiley, New York, 1986).
[25] A. I. Fehrer, F. D. Collins, and T. Healy, Aust. J. Chem. **30**, 511 (1977).
[26] A. D. Williams, J. M. Wilkins, and R. A. Dluhy, Colloids Surf., A **102**, 231 (1995).
[27] DOPG is 1,2-dioleoyl-*sn*-glycero-3-phosphoglycerol; DPPG is 1,2-dipalmitoyl-*sn*-glycero-3-phosphoglycerol.